We are IntechOpen, the world's leading publisher of Open Access books Built by scientists, for scientists

6,900
Open access books available

186,000
International authors and editors

200M
Downloads

154
Countries delivered to

Our authors are among the

TOP 1%
most cited scientists

12.2%
Contributors from top 500 universities

CLARIVATE ANALYTICS
BOOK CITATION INDEX
INDEXED

WEB OF SCIENCE™

Selection of our books indexed in the Book Citation Index
in Web of Science™ Core Collection (BKCI)

Interested in publishing with us?
Contact book.department@intechopen.com

Numbers displayed above are based on latest data collected.
For more information visit www.intechopen.com

Chapter

Solar Pond Driven Air Conditioning Using Seawater Bitterns and MgCl$_2$ as the Desiccant Source

Esam Elsarrag, Opubo N. Igobo and Philip A. Davies

Abstract

Solar energy is used for a wide range of applications such as electricity production, desalination, cooling, heating, etc. Solar-based technologies are widely spread and increasingly studied in the industry. This theoretical and experimental study focuses on solar ponds as a desiccant and low-grade energy source. A thermal model has been developed for a salinity gradient solar pond (SGSP) with a non-convective zone split into 10 sub-zones. A solar pond was constructed and used as a case study for the validation of the predictive model capabilities. The dimensional characteristics of the pond, as well as the solar radiation intensity and ambient temperature data obtained from the meteorological data, were used to produce the solar pond's zone thermal behaviour data. With regards to the thermal behaviour measurements obtained from the solar pond, the predicted data were found to be higher. There is a significant difference between the real-world and meteorological data obtained, the difference between the predicted and real-world pond temperature data was also attributed to the fact that the actual absorbed solar radiation was reduced due to wall shading effect, turbidity and insufficient duration of operation of the pond. In the following year, the stored heat from the previous summer would be expected to improve thermal storage values obtained partially.

Keywords: solar energy, solar pond, desiccant cooling, carbon emissions, humid climates

1. Introduction

The continuous increase in energy demand raises the need for alternative energy sources. Energy consumption from air conditioning will continue to increase which will raise the need for innovative solutions in many industrial sectors. One of the significant sources alternative widely and increasingly studied in the industry is solar-based technologies. Solar energy is used for a wide range of applications such as electricity production, desalination, cooling, heating, etc. Solar ponds are relatively simple and yet effective thermal storage [1].

A solar pond consists of a body of salty water which collects solar energy and converts it for thermal storage. A solar pond can be either convective or non-convective. The principle of convective solar ponds largely depends on the water's

surface being covered by an insulating material to store the system's collected heat; the most commonly used solar pond of this type is the shallow solar pond. Non-convective solar ponds, however, operate by limiting the process of natural convection by the use of a water collector or storage medium.

In this study, a salinity gradient solar pond (SGSP) is designed and constructed. The SGSP is a large, low-cost solar-thermal energy collection and storage system which consists of a large body of saltwater (with salinity gradient) such that solar energy incident on the pond is partially transmitted to the bottom of the pond where a portion (20–30%) of it is absorbed.

A typical SGSP consists of three regions: the upper-convective zone (UCZ), the non-convective zone (UCZ) and the lower-convective zone (LCZ). The UCZ is the topmost layer of the solar pond and is a relatively thin layer (usually 0.1–0.5 m) which contains almost no salinity (about 0–5% concentration). The NCZ is the middle region (of about 0.7–1.5 m thickness) and has an increasing concentration (salinity gradient) relative to the UCZ, and it also acts as insulation on the LCZ, because convection motion in the NCZ is ideally suppressed if the concentration gradient is sufficiently large. The LCZ is the layer in which the salt concentration is the greatest (about 26%), and there is no concentration gradient in it, as depicted in **Figure 1** [3].

Resultantly, large amounts of heat can potentially be stored in these systems [4]. The utilisation of solar ponds as energy carriers was first conceived by Tabor [5, 6] when observing the natural phenomenon in a Hungarian lake at the turn of the twentieth century. The studies proposed the possibility of simulating the natural phenomenon experimentally for energy production. The authors laid the all-important foundations of current solar pond research conducted to date. However, the work of Tabor [6] was not developed as far as its potential would allow. Nevertheless, in recent decades, with the current global search for alternative energy, as aforementioned, solar ponds have gained a substantial increase in interest in academia and industry [1, 3, 7].

A wide variety of models have been developed to investigate the energy proper-ties and potential capabilities of solar ponds. Rabl and Nielsen [4] first examined the possibility of utilising the thermal energy from solar ponds for space heating, by deriving a set of formulae specific to a certain type of salt gradient pond. The pond,
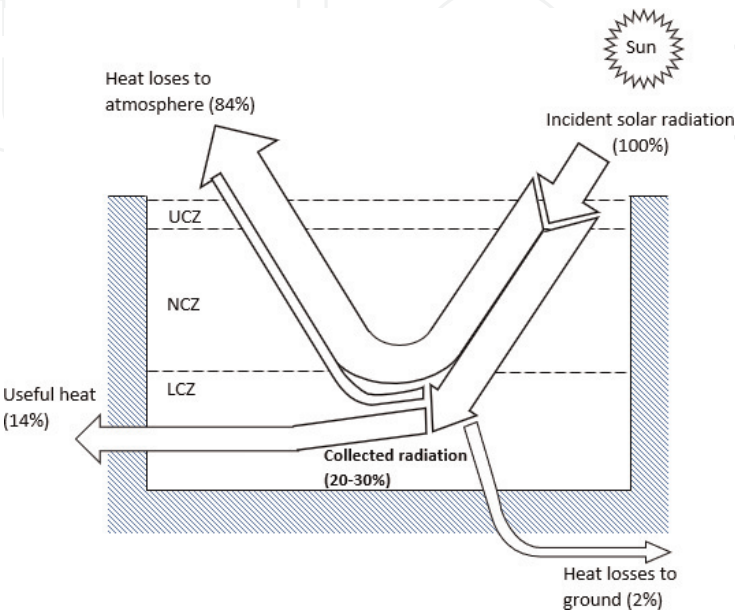

Figure 1.
SGSP solar radiation distribution [2].

in essence, consisted of two homogeneous layers: an upper convecting layer (a lower salt content) and a lower non-convecting layer which acts as the thermal storage part of the pond.

The authors considered the varying temperature ranges that a standard-sized dwelling would encounter seasonally in varying locations and climates. They subsequently reported that the use of a solar pond would undoubtedly provide adequate heating at prices, competitive with those of conventional heating solutions, for the various climates and geographic locations they considered; including the Arctic Circle. Due to its simplified nature, the model developed by Rabl and Nielsen [4] revived solar pond research and had subsequently been used to study the prospects of solar ponds in many regions and climates [8].

Kooi [9] developed an analytical model to study operating characteristics, such as its temperature distributions and energy fluxes, on the assumption that the non-convective zone temperature was equal to the ambient wet-bulb temperature. The model would allow the analysis of the performance of three-layer solar pond systems to be conducted in a similar calculation model to the Hottel-Whillier-Bliss equations [10] used for steady-state flat plate solar energy collectors.

With validation, established models such as that of Rabl and Nielsen [4] deemed the steady-state salt gradient of a solar pond system to be similar to that of a flat plate collector. Kooi [11] also modified the formulae developed by Rabl and Nielsen [4] to account for reflected radiation. He assumed that, since most solar ponds would operate near the solubility limit, this would naturally increase the reflectivity of the solar pond floor. Kooi concluded that the increase of reflectivity, in fact, reduced the efficiency of the steady-state system and that avoidance of supersaturation would be the key for an economical solar pond system.

Other authors also studied the influence of a solar pond's physical properties on its thermal storage efficiency. Wang and Seyed-Yagoobi [12] developed the equations reported by Kooi [11] to investigate the influence of the water's clarity and salt concentrations on the penetration of solar radiation underwater. The authors used turbidity as a parameter for the solar pond's water clarity. The authors reported that solar radiation did not affect the penetration of solar radiation underwater. However, the clarity of the water was found to be imperative, as the turbidity was observed to affect solar radiation penetration with increasing depths.

Karakilcik et al. [13] assessed the performance effect of the presence of shade on each of the solar pond zones. The authors reported a major influence on the solar pond's efficiency caused by the solar pond's shading effect. Another potential performance effect was proposed by Jaefarzadeh and Akbarzadeh [14]. The authors suggested that wind-induced mixing could affect the salinity gradient required for an effectively operating solar pond. The use of floating rings on the surface of the pond would help to mitigate such effects and thus improve performance year-round.

With a great amount of progress focussed on the analysis of the efficiency, performance and adverse effect mitigation, the salt gradient solar pond has been shown by many accounts to be a very promising technology for energy storage that can be adapted to many climates and geographical locations. Elsarrag et al. [15] reviewed the possibility of supplying the necessary energy required for the regeneration stage of a liquid desiccant cooling system using a salt gradient solar pond. The authors considered different solar pond system configurations, designs and solute materials which would be suitable for implementations in a potential solar-powered desiccant cooling system. Sayer et al. [16] researched the feasibility and performance gel pond and compared with the salinity gradient solar pond for low temperature applications. Amro and Yusuf [17] conducted a theoretical study of using solar ponds for seawater desalination in Qatar.

This study aims to investigate theoretically and validate a salt gradient solar pond experimentally as a desiccant and energy source in a hot-humid climate. The model is comprised of energy balances of the pond (including each salt gradient, pond wall, and surface area), saltwater thermo-physical properties and soil temperature.

2. Modelling of a salinity gradient solar pond

The behaviour of a solar pond, like any other solar-thermal collector, is majorly influenced by its geographical location. The pond of interest for the title-study has been constructed and has been analysed for more than 10 months in a hot-humid climate. Initially, the weather data for the location, as obtained from the NASA Atmospheric Science Data Centre at 25.2867°N and 51.5333°E (the geographical location of the salinity gradient solar pond of interest) is given in **Table 1**.

The temperature profile needs to be determined to characterise the thermal behaviour of the pond. The temperature varies with depth (and time). The temperature profile of the solar pond can be obtained from an energy balance of the solar pond. The general energy balance equation is in the form:

$$\begin{pmatrix} rate\ of change \\ of energy\ content \\ of\ elemental\ layer \end{pmatrix} = \begin{pmatrix} rate\ of heat \\ flow \\ into\ the\ element \\ layer \end{pmatrix} + \begin{pmatrix} rate\ of\ heat \\ generation\ in \\ the\ elemental \\ layer \end{pmatrix}$$

$$- \begin{pmatrix} rate\ of\ heat \\ flow \\ out\ from\ the \\ elemental\ layer \end{pmatrix}$$

Month	Insolation (kWh/m^2/day)	$T_{amb,\ av}$ (°C)	V (m/s)	RH (%)
Jan	3.42	19.5	4.11	52.5
Feb	4.25	20.1	4.71	51.8
Mar	4.88	22.5	4.44	51.4
Apr	5.84	26.7	4.12	47.3
May	6.92	31.4	4.52	42.2
Jun	7.4	33.7	4.75	41.7
Jul	7.01	35.2	4.35	42
Aug	6.57	35.4	4.28	43.5
Sep	5.84	33.4	3.83	44.8
Oct	4.84	30	3.5	47.8
Nov	3.78	25.9	3.52	50.2
Dec	3.2	21.9	4.05	52.9

Table 1.
Metrological data for Doha.

Assuming an initial pre-stable ideal state, convection is ideally suppressed in the pond, thus heat flow is primarily by conduction. Thus, the energy balance can be expressed in terms of the one-dimensional heat conduction equation in differential form as:

$$\rho C_p \frac{\partial T}{\partial t} = \frac{\partial}{\partial z}\left(k\frac{\partial T}{\partial z}\right) + \dot{g}(z,t) - L(z,t) \tag{1}$$

where the thermo-physical properties (density, thermal conductivity and specific heat capacity) of the saltwater vary with temperature and concentration. For example, for NaCl pond, the following correlations are widely employed [18]:

$$k = 0.5553 - 0.0000813S + 0.0008(T - 20) \tag{2}$$

$$\rho = 998 + 0.65C - 0.4(T - 20) \tag{3}$$

$$Cp = 4180 + 4.396C + 0.0048S^2 \tag{4}$$

3. Energy analysis of the solar pond

The temperature profile of the solar pond can be obtained from an energy balance of the different zones of the solar pond. With the assumptions that [2]:

- The temperature variation in the horizontal direction is assumed negligible. Thus the temperature and concentration distribution can be considered one-dimensional.

- The three zones of the pond (UCZ, NCZ and LCZ) are considered distinct enough to have a clear fixed boundary.

- The bottom surface of the pond is assumed appropriately blackened; as such the radiation reaching the LCZ is completely absorbed by the saltwater and the pond's bottom.

- Due to the presence of convection in the UCZ and the LCZ, the temperature and concentration in these zones are considered uniformly constant; such that they can be treated as single cells with a thickness *zu* and *zl*, respectively.

- The temperature varies with depth in the NCZ, and as such, in applying the energy balance, this part of the pond can be divided into several imaginary layers, *i* of thickness Δz each.

- The pond is considered very large. Thus, the side effects such as convection current at the wall can be ignored [19].

3.1 Upper-convective zone (UCZ)

Due to convection in the UCZ, it can be treated as having a uniform temperature. The heat balance equation for the UCZ can be given as:

$$Q_{UCZ} = Q_{NU} + Q_{solar} - Q_U \tag{5}$$

$$Q_U = Q_{Uc} + Q_{Ur} + Q_{Ue} + Q_{Us} \tag{6}$$

The solar radiation intensity, I, at a given layer (depth) in the pond can be obtained as a fraction of the radiation that penetrates the pond's surface.
The solar radiation in the pond decays exponentially with depth

$$I_z = \tau I_o \tag{7}$$

The fraction (τ) varies with the depth (z), and can be expressed as:

$$\tau = 0.36 - 0.08 \ln(z) \tag{8}$$

While, the solar radiation that penetrates the pond's surface can be expressed in terms of the incident radiation on the pond's surface; taking into consideration that not all the incident rays penetrate (refracted) at the surface, as some are reflected back.

$$I_o = \beta I \tag{9}$$

$$\beta = 1 - \frac{1}{2}\left[\frac{\sin^2(\theta_i - \theta_r)}{\sin^2(\theta_i + \theta_r)} + \frac{\tan^2(\theta_i - \theta_r)}{\tan^2(\theta_i + \theta_r)}\right] \tag{10}$$

are related to the refractive index, n (=1.33 for water) as:

$$\sin\theta_i = n\sin\theta_r \tag{11}$$

The angle of incidence can be obtained from:

$$\cos\theta_i = \cos\delta\cos\theta\cos\omega + \sin\delta\sin\theta \tag{12}$$

$$\delta = 23.45 \sin\left(\frac{360(284 + N)}{365.25}\right) = 23.45 \sin\left(\frac{360(N - 80)}{370}\right) \tag{13}$$

$$\omega = \frac{2\pi(h - 12)}{24} \text{ (in rad)} \tag{14}$$

$$\omega = \frac{360(h - 12)}{24} \text{ (in degree)} \tag{15}$$

The convective heat loss rate from the pond's surface, $\dot{Q}_{Uc}$ is:

$$\dot{Q}_{Uc} = Ah_c(T_u - T_a) \tag{16}$$

where the convective heat transfer coefficient can be obtained as:

$$h_c = 5.7 + 3.8V \tag{17}$$

The heat loss rate due to radiation $\dot{Q}_{Ur}$ is

$$\dot{Q}_{Ur} = \varepsilon\sigma A\left(T_u{}^4 - T_{sky}{}^4\right) \tag{18}$$

The sky temperature T_{sky} can be determined as:

$$T_{sky} = T_a - \left(0.55 + 0.061\sqrt{P_w}\right)^{0.25} \tag{19}$$

The evaporative heat loss rate $\dot{Q}_{Ue}$ is obtained as:

$$\dot{Q}_{Ue} = \frac{\lambda h_c (P_u - P_w)A}{1.6 C_{p_a} P_{atm}} \tag{20}$$

$$P_u = \exp\left(18.403 - \frac{3885}{T_u + 230}\right) \tag{21}$$

$$P_w = R_H \exp\left(18.403 - \frac{3885}{T_a + 230}\right) \tag{22}$$

$$C_{p_a} = 1.005 + 1.82 Rs \tag{23}$$

The heat loss through the sidewall $\dot{Q}_{Us}$ can be obtained as:

$$\dot{Q}_{Us} = C_w A_{wU}(T_u - T_{GU}) \tag{24}$$

$$C_w = \frac{1}{R_w} = \frac{k_p k_c}{S_p k_c + S_c k_p} \tag{25}$$

The solar energy absorbed by the zone can be obtained as the difference between the radiation entering the zone and the radiation leaving the zone.

With the foregoing, the energy balance equation for the UCZ can be written in differential form as:

$$\rho C_p \frac{\partial T_U}{\partial t} = \frac{\partial}{\partial z}\left(k \frac{\partial T}{\partial z}\right) + \frac{\partial I_{(z,t)}}{\partial z} - \dot{q}_u \tag{26}$$

$$z_1 A \rho C_p \frac{\partial T_U}{\partial t} = kA \frac{\partial T}{\partial z}\bigg|_{z=z_1} + \beta A_{(z_1)} I\left(\tau_{(0,t)} - \tau_{(z_1,t)}\right) - \dot{Q}_u \tag{27}$$

Thus, the heat balance in non-differential form can be written as:

$$z_1 A \rho_u C_{p_u} \frac{T_{U(t+1)} - T_{U(t)}}{\Delta t} = \frac{k_{\frac{1}{2}} A_{\frac{1}{2}}\left(T_{(1,t)} - T_{U(t)}\right)}{\frac{\Delta z_1}{2}} + \beta A_{e(u)} I\left(\tau_{(0,t)} - \tau_{(z_1,t)}\right) - \dot{Q}_{u(t)} \tag{28}$$

Thus, the UCZ layer temperature can be obtained as:

$$T_{U(t+1)} = T_{U(t)} + \frac{\Delta t}{z_u A_u \rho_u C_{p_u}}\left\{\frac{k_{\frac{1}{2}} A_{\frac{1}{2}}\left(T_{(1,t)} - T_{U(t)}\right)}{\frac{\Delta z_1}{2}} + \beta A_{e(u)} I\left(\tau_{(0,t)} - \tau_{(z_1,t)}\right) - \dot{Q}_{u(t)}\right\} \tag{29}$$

3.2 Non-convective zone (NCZ)

The NCZ is assumed to be divided into several imaginary layers i, with the first and last layers having a boundary with the UCZ and LCZ denoted as 1 and f, respectively; thus, the temperature in the first layer can be denoted as T_1 and in the last layer as T_f.

Here, the heat balance for the NCZ can be given as:

$$Q_{(i,t+1)} = Q_{(i+1,t)} + Q_{(solar)} - Q_{(i-1,t)} - Q_{s(i,t)} \tag{30}$$

Thus, the energy balance can be written in differential form as:

$$A\rho_i C_{p_i} \frac{\partial T}{\partial t} = \frac{\partial}{\partial z}\left(kA\frac{\partial T}{\partial z}\right)_{z_{i+1}} + \beta I \frac{\partial\left(A_{e(z)}\tau_{(z)}\right)}{\partial z} - \frac{\partial}{\partial z}\left(kA\frac{\partial T}{\partial z}\right)_{z_{i-1}}$$
$$- C_w \frac{\partial A_{w(z)}}{\partial z}\left(T_{(i,t)} - T_G\right) \tag{31}$$

Or,

$$\Delta z_i A_i \rho_i C_{p_i} \frac{\partial T}{\partial t} = kA\left.\frac{\partial T}{\partial z}\right|_{z=z_{i+1}} + \beta A_{e(i)} I\left(\tau_{\left(i-\frac{1}{2},t\right)} - \tau_{\left(i+\frac{1}{2},t\right)}\right) - kA\left.\frac{\partial T}{\partial z}\right|_{z=z_{i-1}}$$
$$- C_w A_{w(i)}\left(T_{(i,t)} - T_G\right) \tag{32}$$

And in non-differential form:

$$\Delta z_i A_i \rho_i C_{p_i} \frac{T_{(i,t+1)} - T_{(i,t)}}{\Delta t} = \frac{k_{\left(i+\frac{1}{2}\right)}A_{\left(i+\frac{1}{2}\right)}\left(T_{(i+1,t)} - T_{(i,t)}\right)}{\Delta z_i} + \beta A_{e(i)} I\left(\tau_{\left(i-\frac{1}{2},t\right)} - \tau_{\left(i+\frac{1}{2},t\right)}\right)$$
$$- \frac{k_{\left(i-\frac{1}{2}\right)}A_{\left(i-\frac{1}{2}\right)}\left(T_{(i,t)} - T_{(i-1,t)}\right)}{\Delta z_i} - C_w A_{w(i)}\left(T_{(i,t)} - T_G\right) \tag{33}$$

Hence, the temperature of a layer of the NCZ can be expressed as:

$$T_{(i,t+1)} = T_{(i,t)} + \frac{\Delta t}{\Delta z_i A_i \rho_i C_{p_i}}\left\{ \frac{k_{\left(i+\frac{1}{2}\right)}A_{\left(i+\frac{1}{2}\right)}\left(T_{(i+1,t)} - T_{(i,t)}\right)}{\Delta z} \right.$$
$$+ \beta A_{e(i)} I\left(\tau_{\left(i-\frac{1}{2},t\right)} - \tau_{\left(i+\frac{1}{2},t\right)}\right) - \frac{k_{\left(i-\frac{1}{2}\right)}A_{\left(i-\frac{1}{2}\right)}\left(T_{(i,t)} - T_{(i-1,t)}\right)}{\Delta z} \tag{34}$$
$$\left. - C_w A_{w(i)}\left(T_{(i,t)} - T_{G(i)}\right)\right\}$$

3.3 Lower-convective zone (LCZ)

Using the same procedure that outlined previously, the heat balance equation for the LCZ can be expressed as:

$$Q_L = Q_{(solar)} - Q_{L\to N} - Q_{s(i,t)} - Q_G - Q_{ext} \tag{35}$$

$$z_l A_l \rho_l C_{p_l} \frac{\partial T_l}{\partial t} = \beta A_{e(z_3)} I\left(\tau_{(z_3,t)}\right) - kA\left.\frac{\partial T}{\partial z}\right|_{z=z_2} - C_w A_{w(z_l)}\left(T_{(l,t)} - T_G\right)$$
$$- C_{gw} A_{z_3}\left(T_{(l,t)} - T_G\right) - Q_{ext} \tag{36}$$

$$z_l A_l \rho_l C_{p_l} \frac{T_{(l,t+1)} - T_{(l,t)}}{\Delta t} = \beta A_{e(z_3)} I\left(\tau_{(z_3,t)}\right) - \frac{k_l A_{z_2}\left(T_{(l,t)} - T_{(f,t)}\right)}{\frac{\Delta z}{2}}$$
$$- C_w A_{w(z_l)}\left(T_{(l,t)} - T_G\right) - C_{gw} A_{z_3}\left(T_{(l,t)} - T_G\right) - Q_{ext} \tag{37}$$

Thus, the temperature of the LCZ can be given as:

$$T_{(l,t+1)} = T_{(l,t)} + \frac{\Delta t}{z_l A_l \rho_l C_{p_l}}\left\{ \beta A_{e(z_3)} I\left(\tau_{(z_3,t)}\right) - \frac{k_l A_{z_2}\left(T_{(l,t)} - T_{(f,t)}\right)}{\frac{\Delta z}{2}} \right.$$
$$\left. - C_w A_{w(z_l)}\left(T_{(l,t)} - T_G\right) - C_{wg} A_{z_3}\left(T_{(l,t)} - T_G\right) - Q_{ext}\right\} \tag{38}$$

3.4 Dimensions of the solar pond

The dimensional characteristics of each zone of the solar pond would need to be initially ascertained to obtain the temperature predictions of each of the pond's zones. The geometry of the pond could be characterised as shown in **Figure 2**. Here, the relevant cross-sectional surface areas (required for heat transfer) are deduce in relation to the dimensional references of the zones.

3.4.1 Surface areas of the LCZ

The cross-sectional area of the LCZ, A_l may be calculated at mid-plane of the zone (as shown in **Figure 2**).
The average area is:

$$A_l = x_l \cdot w_l \tag{39}$$

where the average length of the pond at the level (measured at mid-level):

$$x_l = X - 2\left(\frac{z_2 + \frac{z_l}{2}}{\tan\vartheta}\right) \tag{40}$$

Similarly, the average width of the pond can be given as:

$$w_l = W - 2\left(\frac{z_2 + \frac{z_l}{2}}{\tan\varphi}\right) \tag{41}$$

Thus, the area is:

$$A_l = \left(X - 2\left(\frac{z_2 + \frac{z}{2}}{\tan\vartheta}\right)\right) \cdot \left(W - 2\left(\frac{z_2 + \frac{z_l}{2}}{\tan\varphi}\right)\right) \tag{42}$$

Similarly,

$$A_{z_2} = \left(X - 2\left(\frac{z_2}{\tan\vartheta}\right)\right) \cdot \left(W - 2\left(\frac{z_2}{\tan\varphi}\right)\right) \tag{43}$$
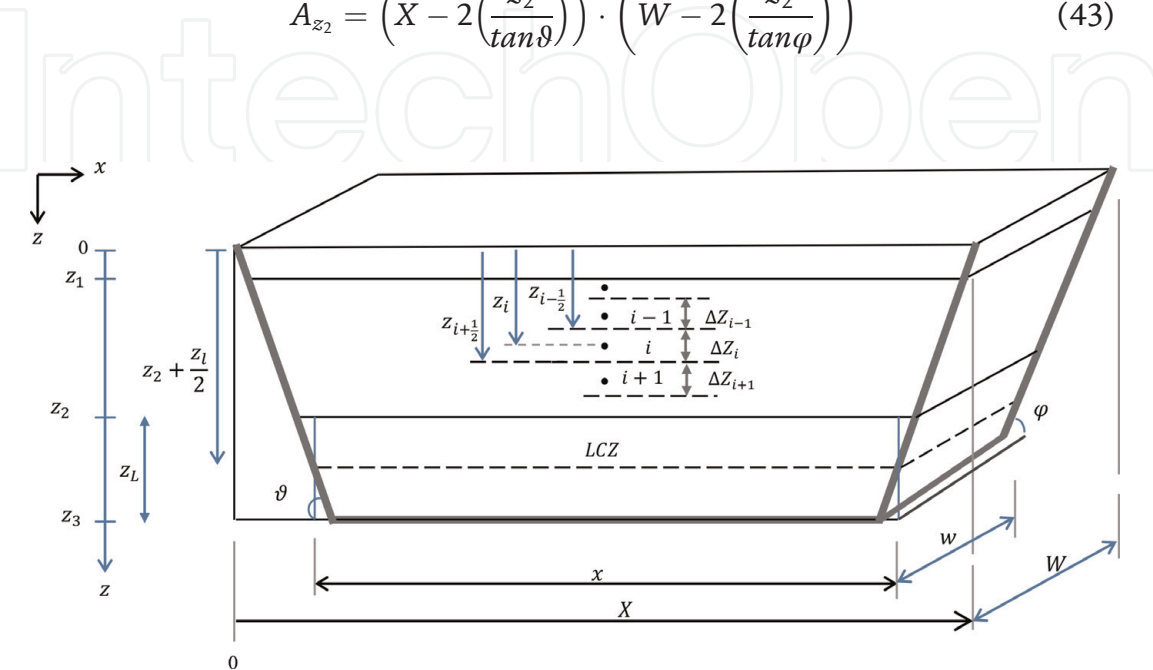

Figure 2
The dimensional characteristics of the solar pond.

Side wall area, $A_{w(z_l)}$,

$$A_{w(z_l)} = 2A_{w(z_l),W} + 2A_{w(z_l),X} \tag{44}$$

The area of one side (along the width) is:

$$A_{w(z_l),W} = \frac{1}{2}\left[\left(W - 2\left(\frac{z_2}{\tan\varphi}\right)\right) + \left(W - 2\left(\frac{z_3}{\tan\varphi}\right)\right)\right]\frac{z_l}{\sin\vartheta} \tag{45}$$

Hence,

$$A_{w(z_l),W} = \frac{z_l}{\sin\vartheta}\left[W - \frac{z_2}{\tan\varphi} - \frac{z_3}{\tan\varphi}\right] \tag{46}$$

Similarly, the area of an adjacent side along the length is:

$$A_{w(z_l),X} = \frac{z_l}{\sin\varphi}\left[X - \frac{z_2}{\tan\vartheta} - \frac{z_3}{\tan\vartheta}\right] \tag{47}$$

Thus, the total area of the four side walls of the LCZ is:

$$A_{w(z_l)} = 2\frac{z_l}{\sin\vartheta}\left[W - \frac{z_2}{\tan\varphi} - \frac{z_3}{\tan\varphi}\right] + 2\frac{z_l}{\sin\varphi}\left[X - \frac{z_2}{\tan\vartheta} - \frac{z_3}{\tan\vartheta}\right] \tag{48}$$

3.4.2 Surface areas of the UCZ

Following the same procedure, the area for the UCZ can be deduced to be:

$$A_u = \left(X - 2\left(\frac{0 + \frac{z_u}{2}}{\tan\vartheta}\right)\right) \cdot \left(W - 2\left(\frac{0 + \frac{z_u}{2}}{\tan\varphi}\right)\right) \tag{49}$$

$$A_u = \left(X - \frac{z_u}{\tan\vartheta}\right) \cdot \left(W - \frac{z_u}{\tan\varphi}\right)$$

Similarly, the total area of the four side walls for the UCZ can be obtained as:

$$A_{w(z_u)} = 2\frac{z_u}{\sin\vartheta}\left[W - \frac{0}{\tan\varphi} - \frac{z_1}{\tan\varphi}\right] + 2\frac{z_u}{\sin\varphi}\left[X - \frac{0}{\tan\vartheta} - \frac{z_1}{\tan\vartheta}\right] \tag{50}$$

$$A_{w(z_u)} = 2\frac{z_u}{\sin\vartheta}\left[W - \frac{z_1}{\tan\varphi}\right] + 2\frac{z_u}{\sin\varphi}\left[X - \frac{z_1}{\tan\vartheta}\right] \tag{51}$$

3.4.3 Surface areas of the NCZ

$$A_i = \left(X - 2\frac{z_i}{\tan\vartheta}\right) \cdot \left(W - 2\frac{z_i}{\tan\varphi}\right) \tag{52}$$

$$A_{i+\frac{1}{2}} = \left(X - 2\frac{z_{i+\frac{1}{2}}}{\tan\vartheta}\right) \cdot \left(W - 2\frac{z_{i+\frac{1}{2}}}{\tan\varphi}\right) \tag{53}$$

$$A_{i-\frac{1}{2}} = \left(X - 2\frac{z_{i-\frac{1}{2}}}{\tan\vartheta}\right) \cdot \left(W - 2\frac{z_{i-\frac{1}{2}}}{\tan\varphi}\right) \tag{54}$$

The total surface area of the four side walls of an elemental layer in the NCZ is:

$$A_{w(\Delta z_i)} = 2\frac{\Delta z_i}{sin\vartheta}\left[W - \frac{z_{i-\frac{1}{2}}}{tan\varphi} - \frac{z_{i+\frac{1}{2}}}{tan\varphi}\right] + 2\frac{\Delta z_i}{sin\varphi}\left[X - \frac{z_{i-\frac{1}{2}}}{tan\vartheta} - \frac{z_{i+\frac{1}{2}}}{tan\vartheta}\right] \qquad (55)$$

where

$$z_i = z_1 + (i-1)\Delta z + \frac{\Delta z}{2} \qquad (56)$$

$$z_{i-\frac{1}{2}} = z_1 + (i-1)\Delta z \qquad (57)$$

$$z_{i+\frac{1}{2}} = z_1 + i\Delta z \qquad (58)$$

3.5. Soil temperature

Although the earth surface temperature at the location can easily be obtained alongside the metrological data; the temperature of the soil varies with depth, as such requires to be calculated separately as a function of depth and time.

The annual variation of the average soil temperature at different depths can be obtained as [20]:

$$T_g(z,t) = \overline{T}_g + A_0 e^{\frac{-z}{d}} \sin\left[\omega(t-t_0) - \frac{z}{d}\right] \qquad (59)$$

$$A_o = \left(T_{g(0)\,max} - T_{g(0)\,min}\right)/2 \qquad (60)$$

$$d = \sqrt{2D_h/\omega} \qquad (61)$$

$$\omega = \frac{2\pi}{365} \qquad (62)$$

4. Calculation procedure

The solar radiation intensity and ambient temperature data were obtained from the meteorological data for Qatar. The calculation was initialised (at time t = 0) by setting the temperature of the various layers of the pond to be equal to the ambient temperature; while setting the initial salinities of the UCZ and LCZ as equal to 2 and 26%, respectively (i.e. assuming that the pond was initially stabilised artificially).

In the sequence of calculation, the parameters—heat transfer coefficients and the properties of the liquid (in the different layers)—are first determined by the initial (ambient) temperature. Then, the obtained liquid properties are employed together with the solar radiation to determine the temperatures of the different layers of the pond at time interval Δt. The temperature of any layer at a time interval is determined with the liquid properties previously obtained with the preceding temperature of that layer. Using the same procedure, the temperatures of the layers for any selected time interval or time of the day can be calculated. In the simulation, the thickness of UCZ, NCZ and LCZ were taken to be 0.2, 1.3 and 0.5 m, respectively.

5. Modelling results

Results were computed by performing energy balances throughout each layer and sub-layer of the pond to achieve accurate temperatures. As the middle NCZ layer has the greatest depth and in turn has the most changes in salinity and density, it had to be divided into more layers. Each layer, as they have different densities,

Month	T_{atm}	T_{UCZ}	T_{LCZ}
January	19.50	19.50	42.36
February	20.10	20.10	51.69
March	22.50	22.50	58.07
April	26.70	26.70	65.63
May	31.40	31.40	74.51
June	33.70	33.70	79.48
July	35.20	35.20	78.65
August	35.40	35.40	76.23
September	33.40	33.40	71.31
October	30.00	30.00	63.98
November	25.90	25.90	55.58
December	21.90	21.90	49.51

Table 2.
Calculated temperatures of the top (UCZ) and bottom (LCZ) layers.

Month	T_{i1}	T_{i2}	T_{i3}	T_{i4}	T_{i5}
January	21.13	23.74	25.96	27.95	29.82
February	22.31	25.95	29.12	32.00	34.73
March	24.98	29.09	32.68	35.94	39.03
April	29.43	33.91	37.78	41.30	44.64
May	34.44	39.38	43.64	47.50	51.17
June	36.93	42.19	46.74	50.87	54.79
July	38.26	43.26	47.59	51.54	55.30
August	38.26	42.96	47.04	50.76	54.29
September	36.05	40.42	44.24	47.73	51.04
October	32.35	36.29	39.75	42.93	45.95
November	27.93	31.38	34.44	37.27	39.96
December	23.78	26.99	29.86	32.51	35.03

Table 3.
Calculated temperatures of the upper half of the middle (NCZ) layer of the salinity gradient solar pond, divided into 10 sub-layers.

loses heat to the layers immediately below and above dissimilarly. A solar pond operating in the geographical area of interest is predicted to reach a maximum temperature of approximately 79.5°C in the summer months with lows of 40°C in the winter. **Tables 2–4** show the diverse temperatures expected with the months of the year based on the energy balance models discussed in the previous section.

6. Empirical validation

Following the predictions obtained from the calculation model, empirical validation would need to be conducted on the solar pond constructed. Thus, the model

calculations reported in this study were simultaneously compared and validated against the temperature gradient data gathered from a salinity gradient solar pond constructed as aforementioned. The solar pond of interest was constructed with the dimensions shown in **Figure 3**.

Month	T_{i6}	T_{i7}	T_{i8}	T_{i9}	T_{i10}
January	31.68	33.61	35.71	38.08	40.80
February	37.42	40.17	43.08	46.24	49.74
March	42.08	45.20	48.48	52.02	55.92
April	47.95	51.35	54.96	58.89	63.24
May	54.82	58.59	62.62	67.02	71.86
June	58.69	62.71	66.99	71.63	76.72
July	59.02	62.84	66.90	71.28	76.06
August	57.79	61.39	65.19	69.30	73.79
September	54.32	57.66	61.18	64.95	69.07
October	48.92	51.93	55.07	58.40	62.02
November	42.60	45.24	47.96	50.83	53.92
December	37.49	39.96	42.48	45.13	47.98

Table 4.
Calculated temperatures of the lower half of the middle (NCZ) layer of the salinity gradient solar pond, divided into 10 sub-layers.
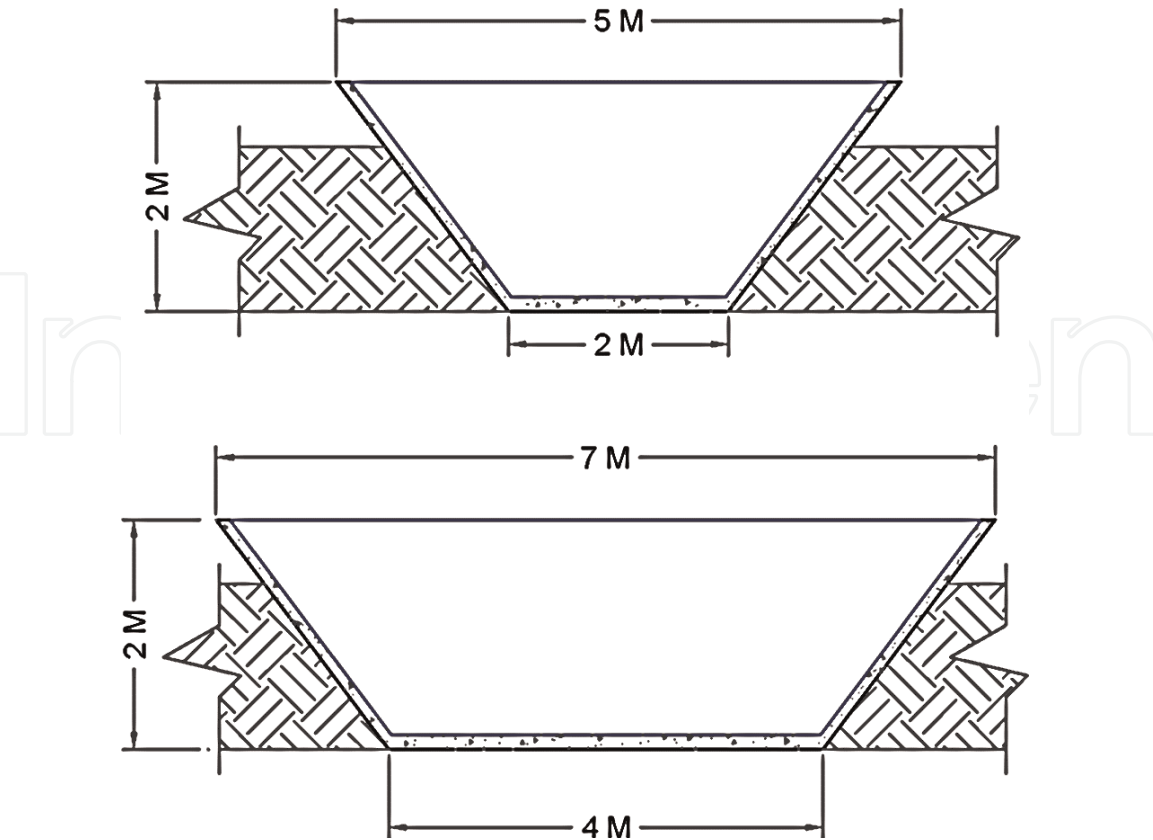

Figure 3
The dimension of the side view (top) and front view (bottom) of the salinity gradient solar pond used for empirical validation of the developed calculation model. The dimensions detailed were used to produce the thermal predictions for the salinity gradient zones of the pond.
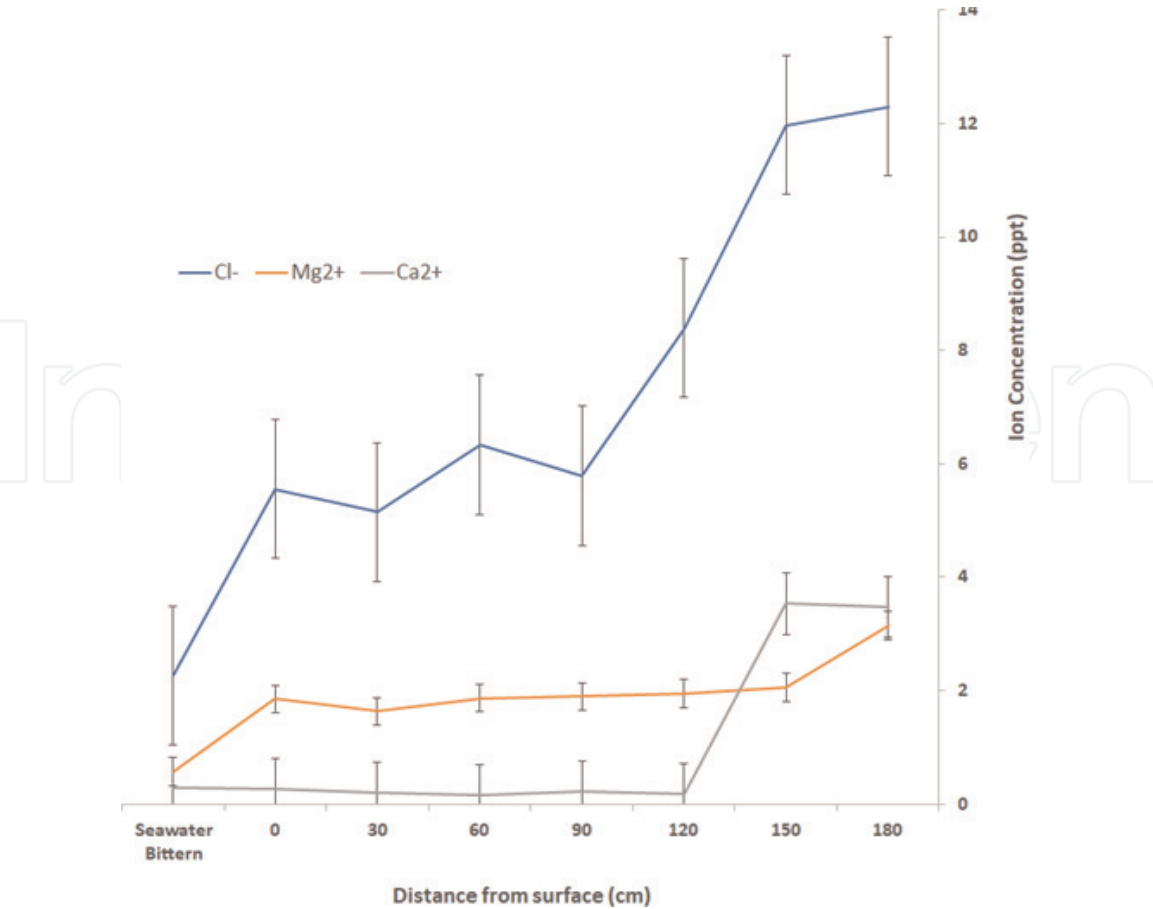
Figure 4
A comparison of the major ion concentration gradient achieved with the constructed solar pond. The samples were obtained using an extraction pump at different depths. The surface data refers to a sample obtained at approximately 5–10 cm below the surface of the pond to allow for the pump to be completely immersed. The bittern sample refers to the ion concentration of the bittern used before the addition of $MgCl_2$.
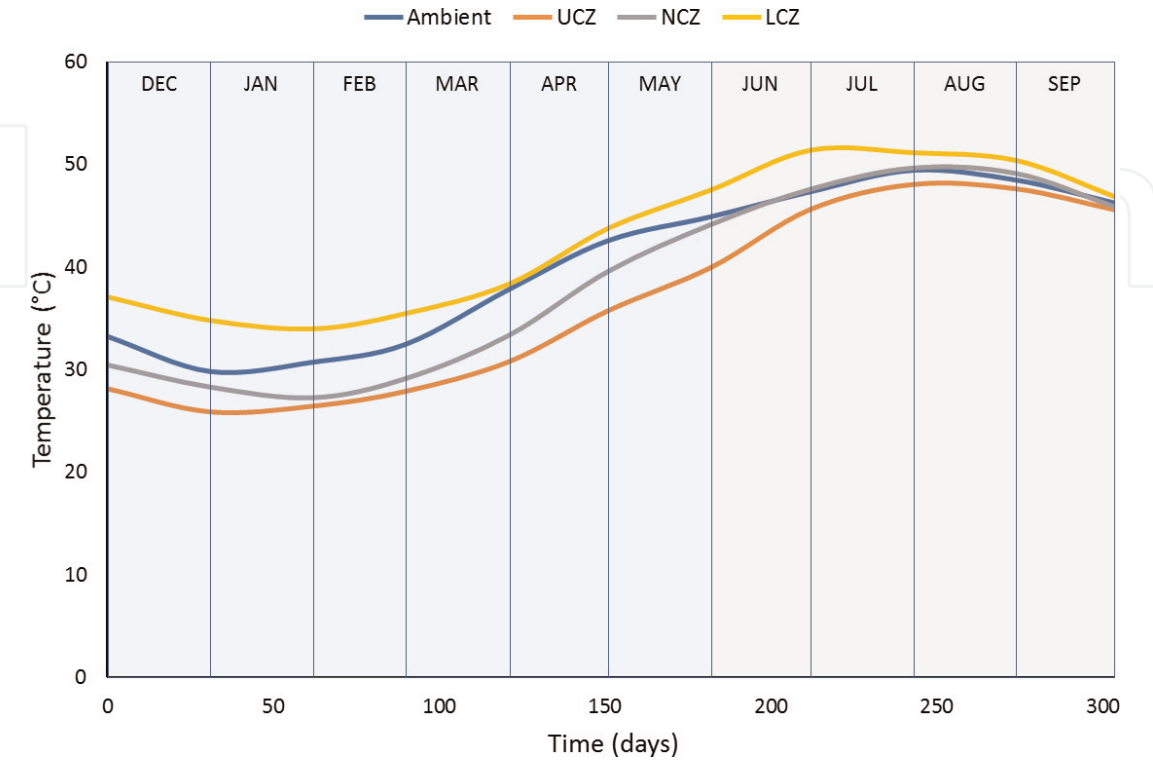

Figure 5
Temperature log of the different zones of the solar pond over the first 300 days of operation. The UCZ, NCZ and LCZ sample were taken at depths of 10, 70 and 150 cm, respectively.
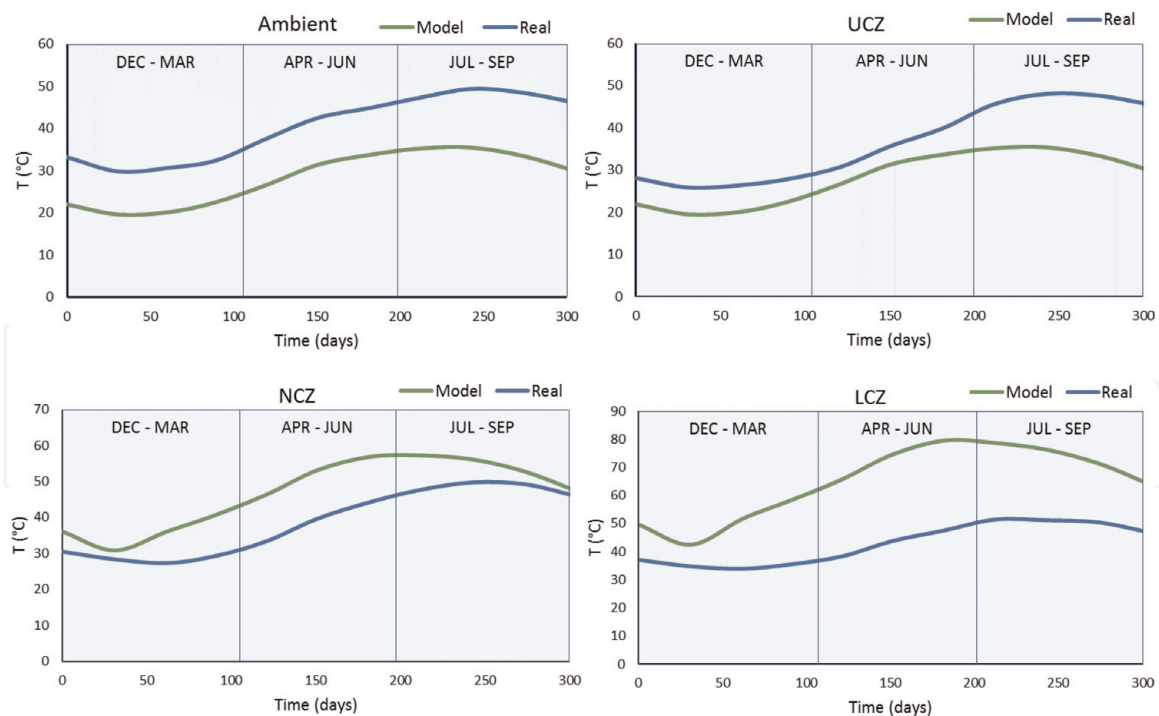
Figure 6
*Comparison of the calculation model predictions vs. the empirical temperature data obtained over the initial 300 days. The NCZ data for the model are the mean values for Ti values reported in **Tables 3** and **4**. The depths of each of the 'real' were obtained at the depths reported in **Figure 5** caption.*

The presence of a well-defined salinity gradient is paramount to the effectiveness of the solar pond's capability for heat storage. Thus, samples were taken at different levels of the pond to observe the concentrations at the expected upper, lower and non-convective zones.

Seawater bittern was the saline material used for the solar pond with additional $MgCl_2$ dissolved in the saline material to ensure a more pronounced salinity gradient was achieved. Future trials were envisioned only to use desalination reject brines as this would not only make use of an industrial waste product, without the conventional energy-intensive processes needed, but it would also improve the potential economic viability of the technology by using an inexpensive resource.

The increase in the salinity of the ponds towards the lower-convective zone can be seen in **Figure 4** and shows promise towards the solar pond's thermal storage potential. An interesting observation of the different ion concentrations were those of calcium and magnesium. The highest concentration cations in the upper and non-convective zones were those of magnesium. It was the case until the deeper depths of the lower-convective zone at which the calcium and magnesium concentrations were much more comparable.

To validate the thermal properties model, the temperatures of the upper-convective, non-convective and lower-convective zones (UCZ, NCZ and LCZ, respectively) were measured periodically as an empirical comparison of the initial 300 days of operation. The temperature measurements were taken at different depths along the centre of the pond; by using RTD with an accuracy of 0.1°C. **Figure 5** shows the temperature measurements obtained from the constructed solar pond while **Figure 6** shows a comparison of the model predictions vs. the actual solar pond temperatures measurements.

The temperature of the lower-convective zone was not expected to reach the heights predicted by the model as the winter month predictions begin with a solar pond with an LCZ already at temperatures of over 45°C stored from the previous summer months. However, the gradual increase in heat storage measured across the

early summer months is promising. Except for the lower-convective zone, the thermal behaviour across the initial months of the solar ponds was increased at a similar rate to the predicted data albeit at lower temperatures. The initial increase was hypothesised to be due to the initial heat of dissolution because of adding the salts to the solar pond.

In a nutshell, though the temperature profile of the pond (through the months of operation) follows a similar pattern to the model predictions, the measured temperatures are lower than predicted. The discrepancy can be partly attributed to the fact that the weather data employed in the model is in variance with the actual weather condition experienced during the pond's operation. In addition, the effects of shading of the side walls and turbidity (clarity of the water) were not considered in the model, but in reality, contribute to the reduction of solar radiation received by the pond. The shading due to the side walls tends to reduce the effective surface area of the pond available to receive incident radiation thus consequently resulting in reduced temperature. The pond is prone to dust (due to the geographical location). Increased dust spread on the pond reduces the clarity of the water thereby reducing the penetration of solar radiation into the pond, consequently reducing the pond temperature.

7. Conclusions

Thermal behaviour analysis and a prediction model have been developed which can be effectively used for the construction and operation of a solar salinity pond. For the developed numerical was split into three sections: the UCZ, NCZ and LCZ. However, the NCZ consisted of a much larger depth than the other zones, thereby resulting in much more significant variance in its salinity and density. It was split into 10 sub-sections. By employing the numerical model in a set calculation procedure, the heat transfer coefficient could be first determined followed by the physical parameter of the pond saline material. Following this procedure, the temperature of each layer (and NCZ sub-layer) could be determined for any period in the year.

In this study, the average temperature of each layer was calculated for each month in the year when exposed to the Qatari temperatures. With the high heat climates of Doha, LCZ temperatures were predicted to reach its highest thermal storage potential at temperatures of about 70°C in June with the lowest in January reaching around 40°C.

The developed numerical model is planned for solar desiccant cooling applications in which the salinity gradient solar pond would be used for thermal storage as well as the storage and regeneration of the liquid desiccant used in the proposed air conditioning system.

Acknowledgements

Nomenclature

$A_{e(i)}$ effective surface area of the layer that receives the solar radiation

$A_{e(u)}$ effective area that receives the solar radiation

$A_{w(i)}$	corresponding surface area of the wall at the given layer
A_{wU}	surface area of side wall corresponding to the UCZ.
C_w	thermal conductance of the composite wall
C_{P_a}	humid heat capacity of air
h	local time
h_c	convective heat transfer coefficient
I	solar radiation intensity
k_p	thermal conductivity of the insulation material
k_c	thermal conductivity of the concrete wall
N	day of the year
P_{atm}	atmospheric pressure
P_u	vapour pressure of water at the upper layer surface temperature
P_w	partial pressure of the water vapour in the ambient air
$\dot{Q}_{ext}$	heat extraction rate (load) from the LCZ by heat exchanger
$\dot{Q}_G$	heat loss rates through the bottom wall (ground) of the pond
Q_{LN}	heat lost from LCZ to NCZ
Q_{NU}	heat gained from NCZ to UCZ
$\dot{Q}_s$	heat loss rates through the side wall of the pond
Q_{solar}	solar energy absorbed by the layer
Q_U	total heat losses from the UCZ
$\dot{Q}_{Uc}$	convective heat loss rate from the pond's surface
$\dot{Q}_{Ue}$	evaporative of heat loss rate
$\dot{Q}_{Ur}$	heat loss rate due to radiation
$\dot{Q}_{Us}$	heat loss through the side wall
R_H	average monthly relative humidity at location
Rs	specific humidity
R_w	total thermal resistance of the individual resistance of the thermal insulation and concrete
RH	relative humidity
S_c	thickness of concrete
S_p	thickness of insulation material
T_1	temperature in the first layer
T_{amb}	ambient air temperature
T_f	temperature in the last layer
$\overline{T_g}$	annual average earth temperature at the location
$T_g(z,t)$	average soil temperature at depth z (m) and time t (d).
$T_{a(n,t)}$	ambient air temperature at time t of nth day of the year
T_{GU}	ground temperature of the surrounding soil at the layer in consideration
T_{sky}	sky temperature.
z_1	depth of the UCZ
ε	emissivity of water
σ	Stefan Boltzmann's constant
V	average monthly wind speed
β	reflectivity of the radiation
θ_i	angle of incidence
θ_r	angle of refraction
Φ	latitude angle
ω	hour angle
δ	declination angle
λ	latent heat of water evaporation
τ	fraction

Author details

Esam Elsarrag[1]*, Opubo N. Igobo[2] and Philip A. Davies[3]

1 BGG, Manchester, UK

2 Howard Butler, Walsall, UK

3 School of Engineering, University of Birmingham, UK

*Address all correspondence to: elsarrag@hotmail.com

IntechOpen

References

[1] Hawlader M. The influence of the extinction coefficient on the effectiveness of solar ponds. Solar Energy. 1980;**25**(5):461-464

[2] Kurt H, Ozkaymak M, Binark AK. Experimental and numerical analysis of sodium-carbonate salt gradient solar-pond performance under simulated solar-radiation. Applied Energy. 2006; **83**(4):324-342

[3] Kurt H, Halici F, Binark AK. Solar pond conception—Experimental and theoretical studies. Energy Conversion and Management. 2000; **41**(9):939-951

[4] Rabl A, Nielsen CE. Solar ponds for space heating. Solar Energy. 1975;**17**(1): 1-12

[5] Tabor H. Solar ponds large-area solar collectors for power production. Solar Energy. 1963;**7**(4):187-188

[6] Tabor H. Non-convecting solar ponds. Philosophical Transactions of the Royal Society of London A: Mathematical, Physical and Engineering Sciences. 1980;**295**(1414):423-433

[7] Bozkurt I, Mantar S, Karakilcik M. A new performance model to determine energy storage efficiencies of a solar pond. Heat and Mass Transfer. 2015; **51**(1):39-48

[8] Bryant H, Colbeck I. A solar pond for London? Solar Energy. 1977;**19**(3): 321-322

[9] Kooi C. The steady state salt gradient solar pond. Solar Energy. 1979;**23**(1): 37-45

[10] Bliss RW. The derivations of several "plate-efficiency factors" useful in the design of flat-plate solar heat collectors. Solar Energy. 1959;**3**(4):55-64

[11] Kooi C. Salt gradient solar pond with reflective bottom: Application to the "saturated" pond. Solar Energy. 1981; **26**(2):113-120

[12] Wang J, Seyed-Yagoobi J. Effect of water turbidity on thermal performance of a salt-gradient solar pond. Solar Energy. 1995;**54**(5):301-308

[13] Karakilcik M, Dincer I, Bozkurt I, Atiz A. Performance assessment of a solar pond with and without shading effect. Energy Conversion and Management. 2013;**65**:98-107

[14] Jaefarzadeh MR, Akbarzadeh A. Towards the design of low maintenance salinity gradient solar ponds. Solar Energy. 2002;**73**(5):375-384

[15] Elsarrag E, Igobo ON, Alhorr Y, Davies PA. Solar pond powered liquid desiccant evaporative cooling. Renewable and Sustainable Energy Reviews. 2016;**58**:124-140

[16] Sayer A, Al-Hussainia H, Campbell A. New comprehensive investigation on the feasibility of the gel solar pond, and a comparison with the salinity gradient solar pond. Applied Thermal Engineering. 2018;**130**(8): 672-683

[17] Amro M, Yusuf B. Integration of pressure retarded osmosis in the solar ponds for desalinationand photo-assisted chloralkali processes: Energy and exergy analysis. Energy Conversion and Management. 2019;**195**:630-640

[18] Kaufmann DW. Sodium Chloride: The Production and Properties of Salt and Brine. New York, USA: Reinhold Publishing; 1960

[19] Ouni M, Guizani A, Lu H, Belghith A. Simulation of the control of a salt gradient solar pond in the south of

Tunisia. Solar Energy. 2003;**75**(2): 95-101

[20] Hillel D. Chapter 12: Soil temperature and heat flow. In: Fundamentals of Soil Physics. New York, USA: Academic Press; 1982. pp. 287-317